Comparing Halide Ligands in PbS Colloidal Quantum Dots for Field-Effect Transistors and Solar Cells

Bederak, Dmytro; Balazs, Daniel M; Sukharevska, Nataliia V; Shulga, Artem G; Abdu-Aguye, Mustapha; Dirin, Dmitry N; Kovalenko, Maksym V; Loi, Maria A

Published in:
ACS Applied Nano Materials

DOI:
10.1021/acsanm.8b01696

Publication date:
2018

ACS APPLIED NANO MATERIALS

Article

Cite This: ACS Appl. Nano Mater. 2018, 1, 6882−6889

www.acsanm.org

Comparing Halide Ligands in PbS Colloidal Quantum Dots for Field-Effect Transistors and Solar Cells

Dmytro Bederak,[†] Daniel M. Balazs,[†] Nataliia V. Sukharevska,[†] Artem G. Shulga,[†] Mustapha Abdu-Aguye,[†] Dmitry N. Dirin,[‡,§] Maksym V. Kovalenko,[‡,§] and Maria A. Loi*[,†]

[†]Zernike Institute for Advanced Materials, University of Groningen, Nijenborgh 4, 9747AG Groningen, The Netherlands

[‡]Department of Chemistry and Applied Biosciences, ETH Zürich, Vladimir Prelog Weg 1, Zürich 8093, Switzerland

[§]Empa-Swiss Federal Laboratories for Materials Science and Technology, Uberlandstrasse 129, Dübendorf 8600, Switzerland

Supporting Information

ABSTRACT: Capping colloidal quantum dots (CQDs) with atomic ligands is a powerful approach to tune their properties and improve the charge carrier transport in CQD solids. Efficient passivation of the CQD surface, which can be achieved with halide ligands, is crucial for application in optoelectronic devices. Heavier halides, i.e., I^- and Br^-, have been thoroughly studied as capping ligands in the last years, but passivation with fluoride ions has not received sufficient consideration. In this work, effective coating of PbS CQDs with fluoride ligands is demonstrated and compared to the results obtained with other halides. The electron mobility in field-effect transistors of PbS CQDs treated with different halides shows an increase with the size of the atomic ligand (from 3.9×10^{-4} $cm^2/(V\ s)$ for fluoride-treated to 2.1×10^{-2} $cm^2/(V\ s)$ for iodide-treated), whereas the hole mobility remains unchanged in the range between 1×10^{-5} $cm^2/(V\ s)$ and $10^{-4} cm^2/(V\ s)$. This leads to a relatively more pronounced p-type behavior of the fluoride- and chloride-treated films compared to the iodide-treated ones. Cl^-- and F^--capped PbS CQDs solids were then implemented as p-type layer in solar cells; these devices showed similar performance to those prepared with 1,2-ethanedithiol in the same function. The relatively stronger p-type character of the fluoride- and chloride-treated PbS CQD films broadens the utility of such materials in optoelectronic devices.

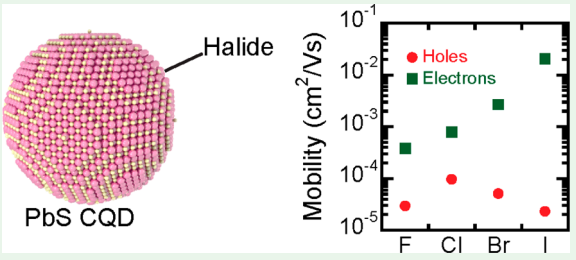

KEYWORDS: *colloidal quantum dots, lead sulfide, halide ligands, charge transport, solar cells*

INTRODUCTION

Colloidal quantum dots (CQDs) are solution-processable semiconductor nanocrystals that have been used to fabricate various optoelectronic devices, such as solar cells, photodetectors, and field-effect transistors.[1] As-synthesized CQDs are capped with long-chain insulating oleic acid ligands to stabilize their colloidal state and passivate their surface. By replacing these bulky native ligands it is possible to enable electronic coupling between the individual quantum dots.

Ideally, the ligand exchange must ensure an efficient passivation of the quantum dot surfaces, preserve quantum confinement, in particular when the CQD solid is used as active layer for solar cells and photodetectors,[2] and allow for rational adjustment of the electronic characteristics (doping levels, carrier mobilities, etc.). Toward these goals, capping CQDs with inorganic ligands received much attention with the introduction of metal chalcogenide complexes.[3] Soon thereafter various small inorganic ligands, such as chalcogenides, halides, pseudohalides, and halometallate complexes showing chemical versatility and providing better processability were introduced for colloidal quantum dot solids.[4−10]

The research on halide ligands is mainly fueled by their prospects in solar cells. Iodide, bromide and chloride have been used intensively as ligands for CQD solids.[6,7,11−14] PbS quantum dot films with Br^- and I^- ligands show n-type transport behavior and exhibit a high degree of surface passivation.[6,11] Furthermore, iodide capping results in exceptionally air-stable n-type CQD solids, which are widely employed as main light absorber layer in CQD solar cells.[15]

The treatment of PbS CQDs with halides results in a short interdot distance favoring good charge transport.[16,17] Fluoride is the smallest ion in the halide series and one of the smallest possible ligands, potentially giving the shortest interdot spacing compared to any other ligand. Despite the prospects, limited attention has been dedicated to the fluoride-treated lead chalcogenide CQDs. Previous reports have mainly focused on the stability of the films toward oxidation based on the study of their optical properties[18,19] The transport properties of fluoride-treated lead chalcogenide CQD films have not been investigated until now.

In this work, the optical and electronic properties of thin films of PbS CQDs treated with the four halide atomic ligands

Received: September 26, 2018
Accepted: November 9, 2018
Published: November 9, 2018

are compared. Not only is the fluoride ligand introduced for the fabrication of PbS CQD devices but its performance is also compared with the other three halide ligands in a homogeneous set of experiments. The properties of the halide-treated films are found to obey a trend-wise dependence on the ligand size. The fluoride-treated sample displays the lowest electron mobility, which increases 2 orders of magnitude moving down in the periodic table (F−Cl−Br−I). Interestingly, the hole mobility for all the halides remains roughly the same. Moreover, in the fluoride-treated PbS quantum dot transistors we observe a time-dependent decreasing of the electron current, suggesting a high sensitivity of this active layer to the traces of contaminants in the glovebox. Quasi-pn junction solar cells were fabricated by replacing the conventional 1,2-ethanedithiol (EDT)-capped CQDs by chloride- or fluoride-treated PbS CQDs, making use of their relative p-type behavior, while keeping the iodide-treated CQDs as main absorber and n-type layer. Halides are less toxic and more environmental friendly than thiols, therefore are more compatible with an eventual industrialization of the process. Solar cells fabricated with fully halide-treated films show power conversion efficiency similar to that of devices using an EDT-treated layer, therefore showing their prospects as solar cell material.

RESULTS AND DISCUSSION

In a few reports, treatment of lead chalcogenide quantum dots with fluoride was performed by using tetrabutylammonium fluoride (TBAF).[18,20] Tetrabutylammonium halide salts are typically available in high purity, setting them favorable for photovoltaic research. Unlike other tetrabutylammonium halides, dried TBAF is reported to decompose at room temperature by Hofmann elimination;[21] hence TBAF is only available in hydrated form or in a solution of water or tetrahydrofuran.[22] The exposure of CQDs to humidity is known to have a significant influence on the material properties,[23−25] making a hydrated fluoride source rather undesirable. Anhydrous TBAF can be generated in situ from the reaction of hexafluorobenzene with tetrabutylammonium cyanide and used for synthetic purposes, but the experimental conditions are rather incompatible with the use in CQD solids.[26] Consequently, an anhydrous fluoride compound that can contend tetrabutylammonium halide series is required for a good comparison between the different halide-treated CQD films. Herein, a tetramethylammonium fluoride is chosen as the source for the fluoride atomic passivation due to its simplicity and facile preparation in anhydrous form.[21] Thus, four anhydrous tetraalkylammonium halide salts, namely tetramethylammonium fluoride (TMAF), tetrabutylammonium chloride (TBACl), tetrabutylammonium bromide (TBABr) and tetrabutylammonium iodide (TBAI), were used for the solid-state ligand exchange. The ligand exchange and the chemicals used in this work are schematically illustrated in Figure 1A.

CQDs with the size between 2.7 and 3.5 nm diameter, as calculated from the first excitonic peak energy of the absorbance spectrum, were used for all the experiments.[27] Thin films of PbS quantum dots treated with the four halides were prepared by spin-coating with subsequent ligand exchange and washing, using the layer-by-layer approach reported earlier.[28] Samples for electron microscopy were prepared by drop-casting on carbon-coated copper grids, the ligand exchange and washing were performed as for the device

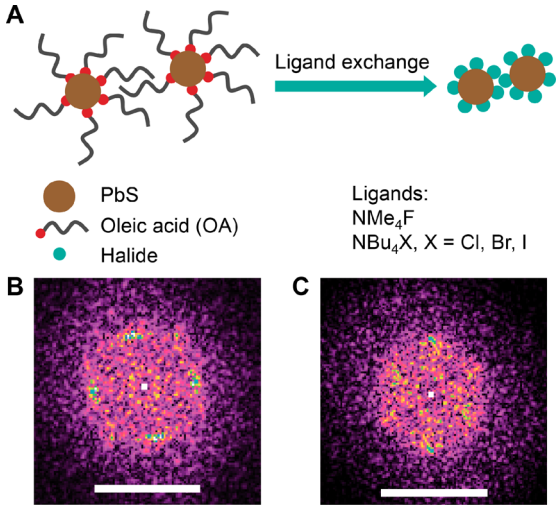

Figure 1. (A) Schematic illustration of PbS colloidal quantum dots with native oleic acid ligands and, after the ligand exchange, with halide ligands. Fourier-transformed TEM images of single CQD domains treated with (B) TBAI and (C) TMAF. The scale bars are 500 μm^{-1}.

fabrication. More details on the sample preparation are reported in the Experimental Methods section.

Smaller PbS CQDs, ca. 3 nm in diameter, have a truncated octahedron shape, mostly dominated by {111} facets, whereas larger PbS particles have cuboctahedron shape with {111} and {100} facets.[29] The variation in faceting creates a significant difference in chemical reactivity and assembly of the CQDs. Larger lead chalcogenide CQDs, of size from 3.8 to 6 nm typically form square superlattices after halide treatment,[16,30] while, in general, smaller CQDs give rise to arrays with a much higher level of disorder. However, such "small" particles attract keen interest because of their application in CQD solar cells. In this work, a relatively large CQD size (3.5 nm) was chosen in order to show the effect of halide treatment on their assembly, whereas smaller particles were used for device fabrication.

Figure 1 illustrates the difference in the CQDs ordering after the ligand exchange with iodide (panel (B)) and fluoride (panel (C)) ligands. The typical square superlattice is observed after the iodide treatment of CQDs with cuboctahedron shape, but domains with hexagonal packing are also present.[16] Ligand exchange with F results in a predominantly hexagonal ordering (Figure 1C) with pronounced disorder. A similar behavior, with a different degree of disorder is found in bromide- and chloride-treated samples (Figure S1). The distance between the single CQDs clearly indicates that the ligand exchange took place also when fluoride ligands are used. Moreover, the presence of fluorine in the ligand-exchanged films is observed using energy-dispersive X-ray spectroscopy (EDX) as reported in Figure S4. However, EDX has low sensitivity to light elements, such as fluorine. Therefore, the detection of fluorine in the sample containing a high amount of heavy atoms suggests a significant fluorine concentration in the thin film.

Electron diffraction patterns of the PbS CQDs treated with TBAI and TMAF are shown in Figure S2. The lack of some of the reflections in the TBAI-treated sample indicates a dominant out-of-plane orientation of the individual CQDs with their {100} facets normal to the surface. Moreover, a preferential in-plane orientation with the neighboring CQDs aligning with their {100} facets facing each other is also

DOI: 10.1021/acsanm.8b01696
ACS Appl. Nano Mater. 2018, 1, 6882−6889

observed as four dominant peaks in the innermost ring. Such organization is not observed in the F^--treated sample, in which all expected reflections are observable as rings, confirming the qualitatively observed disorder of these films.

The average interdot distance is extracted from the Fourier-transformed TEM images of single domains. No clear difference is observed between the fluoride- and iodide-treated samples due to the high level of disorder. The average center-to-center interdot spacing in all halide-capped samples is 4.5 nm, whereas the oleate-capped CQDs show a 4.9 nm periodicity. The reduction of the interdot distance after the halide treatment is a further confirmation of the removal of the long oleate ligands.

Figure 2 shows the optical properties of thin films treated with the four halide ligands, and of an oleate-capped CQD film

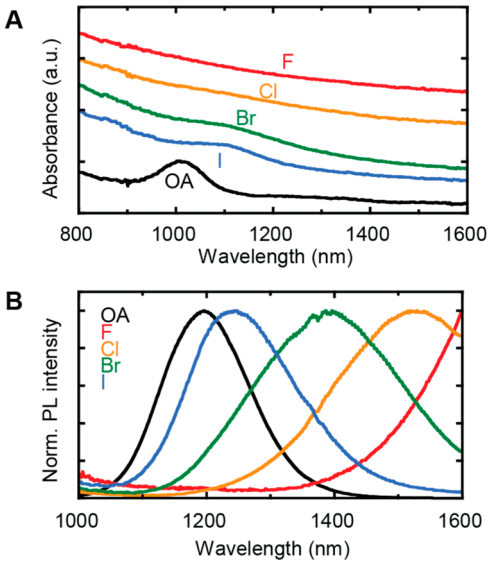

Figure 2. (A) Absorbance spectra of thin films of 3.5 nm PbS CQDs capped with native oleic acid (OA) and with the four halide ligands; the curves are vertically shifted for clarity. (B) Normalized PL spectra of the same films reported in A.

as reference. The absorbance spectra (Figure 2A) show a trend in the degree of confinement. In general, the first excitonic peak shifts toward higher wavelengths, and becomes broader upon ligand exchange with halides. A clear peak is observable only in PbS-I and PbS-Br samples, and not in the PbS-Cl and PbS-F ones. The different energies of the peak (OA < I < Br) are attributed to a ligand-dependent loss of quantum confinement and overlap of the electronic wave functions of individual CQDs in the film. The variation of peak widths (and most likely the lack of excitonic features in the PbS-Cl and PbS-F samples) are signs of increased inhomogeneous coupling due to disorder as observed also in the TEM micrographs. Figure 2B shows the normalized steady-state photoluminescence (PL) spectra of the same samples. All halide-treated samples show a red-shifted emission peak compared to the pristine films, indicating again the increased electronic coupling between CQDs. The red shift of the PL spectra increases from iodide- to fluoride-treated films in the order I < Br < Cl < F, and is in line with the trend observed in the absorption spectra. Although we do not observe a trend-wise dependence of the average interdot spacing on the ligand size, the trend in the spectral features suggests that the effective confinement set by the local interdot spacing and dielectric environment changes.

The broadening of the PL signal confirms the presence of energetic disorder in the halide-treated CQD films, and suggests that the spreading in the absorption peak position is responsible for the lack of the excitonic feature of the Cl^- and F^--treated samples. The PL peak position of the fluoride-treated sample is not visible due to the cutoff of the detector at ~1600 nm, for this reason measurements were repeated using PbS CQDs with higher band gap (3.0 nm size). In this PbS-F sample, a large variation between the PL spectra taken at different spots is observed (examples are shown in Figure S3), confirming the significant inhomogeneity of films obtained with the fluoride ligand.

The ligand exchange process inevitably increases the disorder as the interdot spacing decreases. The degree of positional disorder leads to energetic disorder, which is observed to vary between different samples. The smaller the ligand, the larger the shrinkage of the interdot distance allowing for larger positional disorder. Moreover, the different kinetics of the reactions of the PbS surface with the ligands is coresponsible for the positional disorder.[16] The inhomogeneity and broad PL peak observed in the fluoride samples, and the lack of nanoscale ordering from the electron diffraction patterns are in complete agreement with these arguments.

It was shown in some previous reports that quantum confinement is preserved in Cl^-, Br^-, and I^--capped PbS CQDs films after the solid state ligand exchange.[6] Well-defined excitonic peaks were observed in absorption spectra as well as a minor red shift between the samples treated with different halides. We believe, the discrepancy with our results is caused by the different protocol used for CQD film fabrication, which at parity of concentration could alter the reactivity of the ligands. In particular experiments in ref 6 were performed in ambient condition while ours are performed in inert atmosphere inside a nitrogen-filled glovebox.[10] Another significant difference to underline is that we use thermal annealing for all the samples used for the UV−vis and PL measurements, and for field-effect transistors. This is an important step to obtain well-performing devices. We have seen earlier that our fabrication protocol leads to higher ligand exchange efficiency than reported in other works.[16]

Field-effect transistors (FETs) are powerful tools to study electronic properties of semiconducting materials, to understand the degree of coupling between CQDs induced by the ligands, and to test their quality. Figure 3A shows the schematic structure of the bottom-gate bottom-contact field-effect transistor used in this work. The details of the structure, the fabrication and measurements can be found in the Experimental Methods section.

The transfer characteristics of the FETs are shown in the Figure 3B. All transistors show ambipolar transport; however, with the dominance of the negatively charged carriers. The electron current increases 2 orders of magnitude moving down the group in the periodic table (F−Cl−Br−I), whereas the hole current for all the halide-treated CQD transistors is approximately the same. The extracted charge carrier mobilities are in line with the observed trends for the current in the transfer curves (Figure 3C). The electron mobility has a value of 2.1×10^{-2} $cm^2/(V\ s)$ for PbS-I, 2.7×10^{-3} $cm^2/(V\ s)$ for PbS-Br, and 8.0×10^{-4} $cm^2/(V\ s)$ for PbS-Cl, in a good agreement with previously reported values.[12,16] It is important

DOI: 10.1021/acsanm.8b01696
ACS Appl. Nano Mater. 2018, 1, 6882−6889

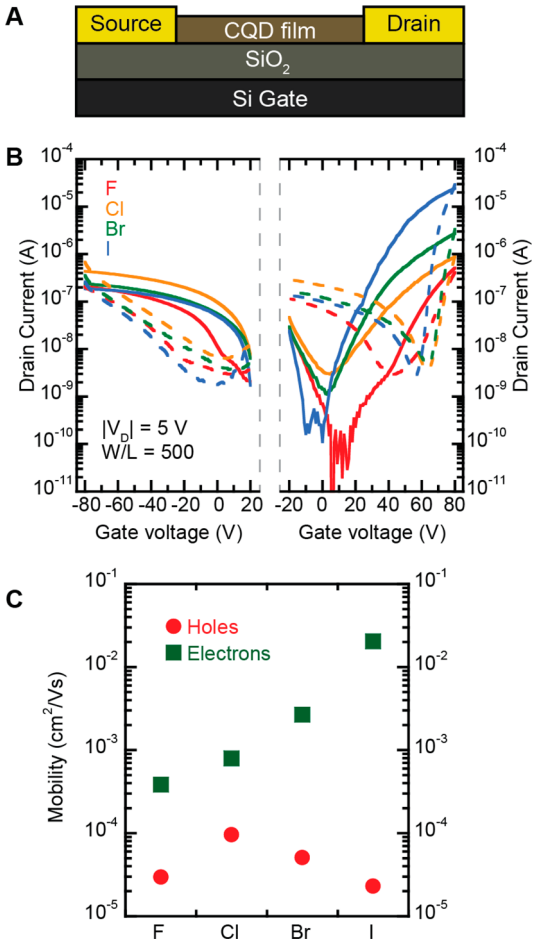

Figure 3. (A) Schematic structure of a PbS CQD FET; (B) transfer characteristics for the p- and n-channel operation of PbS CQD FETs prepared with different halide ligands with the solid lines representing the forward scan and the dashed lines the reverse scans (the color indicates the sample as described in the left panel); (C) comparison of the linear mobility values extracted from the transfer curves.

to note that the fluoride-based sample, which is reported for the first time, fits in the trend.

The influence of the halide ligands on the hole current is less pronounced than on the electron current, the hole mobility values are within the same order of magnitude for all samples (below 1×10^{-4} cm^2/(V s)). The PbS-F device exhibits a fairly balanced transport compared to the typical electron–hole asymmetry of the n-type TBAI or p-type NaSH-treated samples,[31] with $\mu_h = 3.0 \times 10^{-5}$ cm^2/(V s) and $\mu_e = 3.9 \times 10^{-4}$ cm^2/(V s). The variation in the linear mobility values of the PbS-F samples is shown in Figure S6; the spread is larger than for the other samples but within 1 order of magnitude.

It is important to point out that the trend observed in the electron mobilities is against the common assumption that smaller halides should lead to better coupling and therefore better transport. The red-shift of the PL emission peaks suggest that the coupling energy increases from I to F, whereas the electron mobility increases from F to I. Instead, the peak width shows a similar trend of the electron mobility, suggesting that the electron transport in these films is limited by energetic disorder, or in other words the possibility of carrier localization in highly coupled domains, in agreement with previous reports.[32,33] An alternative explanation for the trend of the electron mobility could evoke a different contribution of the ligands to the density of states of the CQD film or to a shift of the Fermi level induced by the ligands.[16]

On the other hand, the hole mobility increases from I to Cl, suggesting a coupling-limited transport. In line with previous observations and reports, the holes are more confined to the CQD cores in off-stoichiometric particles due to the lead-dominated surface providing a larger wave function delocalization for states above the Fermi-level.[31,34] Alternatively a shift of the Fermi level could be also a possible explanation for this trend.

The values of the threshold voltages for PbS-F FETs and the other halide-treated devices are dramatically different. For PbS-F the threshold voltages for holes and electrons are 15 and 62 V, respectively, whereas in the case of Cl^-, Br^- and I^--treated samples, the threshold are approximately equal to 40 V for holes and 50 V for electrons. The higher threshold voltage for electrons and holes in PbS-F is an indication of a more pronounced charge carrier trapping than in the case of the other samples.

A diminishing electron current in PbS-F devices was observed during measurements (Figure S5). This is typically the sign of a high sensitivity of the CQD solids to traces of contaminants in the glovebox (for example O_2 or H_2O),[35] which may be due to a different ability of the halides to protect the inorganic PbS core and the exposure of dangling bonds after the F^- treatment. In fact, the ligands have to form a compact and robust shell on the CQD surface to sterically inhibit the attack of oxygen or water. The iodide shell has been shown to protect the PbS CQDs upon air exposure, and PbS-I CQD solid retains the n-type properties even in air.[11] In contrast, bromide- and chloride-capped CQDs switch polarity after air exposure. The fluoride ligand is the smallest of the halide family and therefore does not provide a good steric screening of the lead chalcogenide core to inhibit the attack of oxidative species; oxidation of fluoride-treated lead chalcogenide CQD films has been proven earlier by spectroscopic studies.[18,19] Another possible explanation of the large instability of the fluoride-treated samples is related to the protic attack of MeOH on the CQD surface followed by desorption of halide ligands. It has been reported that the kinetic energy of the ligand desorption upon the attack of protons changes in the order OA < Cl < Br < I,[11] consistently with the Pearson hard–soft acid–base concept. Fluoride is a hard Lewis base and is "harder" than chloride, thus making more labile bonding with the rather soft Pb ions. Therefore, the desorption energy of the fluoride from the PbS CQD surface should be lower than for chloride. The washing step with a protic solvent (MeOH) can partially remove fluoride from the CQD surface and thus leading to an increased susceptibility of the inorganic PbS core toward oxidation and the formation of traps, which are especially active toward holes. This is consistent with the behavior of the threshold voltage in the p-type transfer characteristics (Figure 3B).

Unfortunately, using acetonitrile as an aprotic solvent was problematic. The issue is that acetonitrile is not compatible with anhydrous fluoride salts[36] and therefore cannot be used for all four halides. The observations from the experiments might be greatly complicated by formation of trans-3-amino-2-butenenitrile from the reaction between fluoride and acetonitrile close to the CQD surface.[21] The acetonitrile solution of TMAF turned yellowish upon dissolving of the white TMAF powder, which shows that the above-mentioned

DOI: 10.1021/acsanm.8b01696
ACS Appl. Nano Mater. 2018, 1, 6882–6889

reaction between fluoride and acetonitrile is fast and occurs at room temperature.

For CQD solar cells, the lack of p-type materials with high doping has been recently identified as a performance limiting factor,[37] and improvements in the device performance have been made by doping the p-type layer in the typical quasi-pn junction device architecture.[38,39] Air sensitivity has been reported to lead to a more pronounced p-type behavior in thiol-capped CQDs,[23] and for this reason they became the most employed ligands for p-type layer for CQDs solar cells. However, halide salts are much better because of their low volatility and toxicity, and, in general, halides give rise to larger environmental stability to the CQD layers.[15] Here, we investigate the ability of PbS-F and PbS-Cl to serve as a p-type layer for CQD solar cells, forming fully inorganic PbS CQD devices. Moreover, the elimination of environmentally unfriendly and difficult to handle thiol-based ligands is an important step in the development of CQD devices.

Solar cells based on the widely used quasi-pn junction architecture, where the layer of PbS treated with 1,2-ethanedithiol (EDT) of the original structure is replaced by fluoride- or chloride-treated layers, are fabricated.[11,15,40] Figure 4A shows the performance of CQD solar cells with the different quasi p-type layers under AM1.5G illumination. The devices using fluoride or chloride ligands for the p-type layer results in a very high short-circuit current density (J_{sc}) of 28.8 and 27.3 mA/cm^2, respectively. The high J_{sc} can be explained by a good energy level alignment and by the ability of the PbS layers treated with small halides to block electrons. Notably, our solar cells with only halide-capped CQDs possess higher J_{sc} than devices using the PbS-I/PbS-EDT structure, indicating that PbS-Cl and PbS-F can play similar role to PbS-EDT determining the energy band bending. This is in line with the trend expected for the energy levels of PbS with these ligands.[20]

The open-circuit voltage (V_{oc}) of the halides-treated p-type layer is 0.51 V, which is lower than the 0.55 V measured for devices obtained with EDT-treated CQDs. The lower V_{oc} of the devices fabricated with halide-treated p-type layers could be attributed to a higher amount of trap states, which increase the nonradiative recombination, or to the decreased band gap of the CQDs.[41] The values of the fill factor (FF) are 0.50 for the device with PbS-F, 0.53 for device with PbS-Cl, and 0.51 for the PbS-EDT reference. The power conversion efficiency (PCE) for all three devices exceeds 7% and does not significantly changes between the different types of samples. However, as explained above the partial figure of merit of these devices (V_{oc}, FF, and J_{sc}) account for the different physical properties. The table in Figure 4C summarizes the device performances for p-type layers obtained with different ligands. Table S1 includes the average and standard deviation for the fabricated devices.

Figure 4B shows the external quantum efficiency (EQE) spectra of the solar cells with different p-type layers. The J_{sc} values obtained from the integration of the EQE spectra are 23.7 mA/cm^2 for devices using EDT ligands, 22.5 mA/cm^2 for devices using Cl and 24.2 mA/cm^2 for the one using F. Obviously, the values of the J_{sc} calculated from the EQE spectra do not perfectly correlate with the J_{sc} from the $J-V$ measurements. A possible source of inconsistency is the low intensity of the light used for the EQE measurements combined with the large absorption of the layers, however, even when the EQE spectra are measured with light bias the discrepancy in the J_{sc} remains. The most important discrepancy between the EQE spectra of the three types of devices is occurring between 400 and 650 nm. This large difference could be determined by the different distribution of the electric field within the active layer determined by the variation of the band gap of the different p-type layers and by the dissimilar transport properties of the studied films.

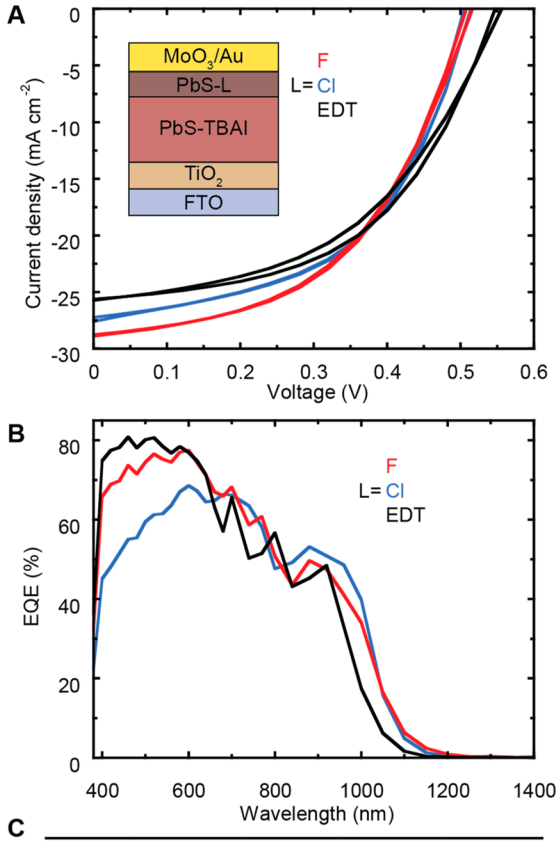

C

L	J_{sc} (mA/cm^2)	V_{oc} (V)	FF	PCE (%)
TMAF	28.8	0.51	0.50	7.4
TBACl	27.3	0.51	0.53	7.3
EDT	25.6	0.55	0.51	7.2

Figure 4. (A) $J-V$ characteristics of the PbS CQD solar cells under AM1.5G illumination, forward and reverse scan directions are plotted in order to show the sample hysteresis. PbS treated with three ligands, namely TMAF, TBACl, and EDT are reported as p-type layers. Inset: CQD solar cell structure used in this work. (B) EQE spectra of the same devices reported in A. (C) Device performances of PbS CQDs solar cells with different p-type layers.

CONCLUSIONS

In conclusion, we compared the treatment of PbS CQDs with all four halides and studied optical and electronic transport properties of the resultant films. For a proper comparison, we introduced tetramethylammonium fluoride as a new anhydrous source of fluoride ligands for CQDs. We found that the fluoride ligand exchange takes place, and a trend-wise dependence between the degree of quantum confinement on the choice of halide ligand is measured. A larger disorder is observed for CQDs treated with F and Cl ligands.

The field effect electron mobility increases with the ligand size while the hole mobility remains approximately the same

DOI: 10.1021/acsanm.8b01696
ACS Appl. Nano Mater. 2018, 1, 6882−6889

for all the halide-treated CQDs. The comparison of the trends in mobility and the red-shift and broadening of the photoluminescence emission spectra suggest that the electron transport is disorder-limited, while the coupling energy is one of the factors determining the hole mobility. The different trends lead to, in proportion, larger p-type behavior of the fluoride- and chloride-treated films compared to the iodide-treated ones.

Finally, we successfully implemented quantum dot film treated with chloride and fluoride as a p-type layer in CQD solar cells. These fully inorganic solar cells showed similar power conversion efficiency to devices fabricated with EDT-treated CQDs as a p-type layer. The possibility to exclude thiols such as EDT in the fabrication process is very important for the possible industrialization of CQD solar cells.

EXPERIMENTAL SECTION

Materials and Reagents. All the solvents and reagents were analytically pure and were used without further purification. Lead(II) acetate trihydrate ($Pb(CH_3COO)_2 \times 3H_2O$, ≥ 99.99%), bis-(trimethylsilyl)sulfide (TMS_2S), 1-octadecene (ODE, 90%), oleic acid (90%), tetrabutylammonium chloride (TBACl), bromide (TBABr) and iodide (TBAI) were purchased from Sigma-Aldrich. Anhydrous tetramethylammonium fluoride (TMAF) was purchased from ABCR. PbS colloidal quantum dots were prepared according to the method of Hines et al.,[42] with slight modifications. Pb-$(CH_3COO)_2 \times 3H_2O$ (1.5 g, 4 mmol), ODE (47 mL), and oleic acid (2.8−3.2 mL, depending on the desired size of final CQDs) were mixed in a three-neck flask. The mixture was degassed under vacuum at 120 °C for 1 h. After that temperature was stabilized at 90−140 °C (depending on the desired size of final CQDs) under nitrogen flow. The heating mantle was removed and solution of TMS_2S (0.42 mL, 2 mmol) in 10 mL of ODE (dried) was injected into vigorously stirring lead oleate solution. After 5 min, the reaction mixture was cooled down to room temperature. NCs were washed three times with toluene/ethanol solvent/nonsolvent pair, redissolved in hexane and filtered through 0.2 μm PTFE filter.

PbS CQD Thin Film Field-Effect Transistor (FET) Fabrication and Measurements. The CQD field-effect transistors were fabricated on top of highly doped Si substrates covered with a 230 nm thermally grown SiO_2 dielectric. Prepatterned interdigitated electrodes consist of 10 nm ITO and 30 nm of Au are served as a source and a drain with a channel width of 10 mm and length of 20 μm. The substrates were cleaned by sonication in acetone and isopropanol and dried in the oven. The CQD films were deposited by a layer-by-layer approach using a modified method from Shulga et al.[28] Namely, the "scaffold" layer was spin-coated at 1000 rpm from 1 mg/mL solution of OA-capped CQDs in hexane. The solid-state ligand exchange was performed with a 20 mM solution of tetraalkylammonium halide in MeOH and the film was washed twice with pure MeOH. This concentration of halide ligand is similar or slightly lower than what could be considered as standard in the field.[6,15] The "filler" layer of CQDs was spin-coated from 5 mg/mL solution. The substrate was dried for the 20 s at 120 °C on a hot plate after each CQDs deposition and ligand exchange step. The devices were annealed after the fabrication for 20 min at 120 °C. All transistor measurements were performed with Agilent E5262A semiconductor parameter analyzer. All fabrication and measurement steps were performed in a N_2-filled gloveboxes with O_2 and H_2O concentration below 0.1 ppm. The hole and electron mobility values were extracted from the transfer (I_D-V_G) characteristics of the FETs in the linear regime using the gradual channel approximation and the parallel plate capacitance of the oxide layer. No obvious Schottky barrier was observed between ITO/Au electrodes and CQD film in the output curves, suggesting limited effect of the contacts on the linear mobility.

Absorbance and PL Measurements. Samples for absorbance and PL measurements were fabricated on quartz substrates using the above-mentioned procedure. The samples were annealed after the fabrication for 20 min at 120 °C. Absorption spectra were recorded using a dual-beam Shimadzu UV-3600 spectrometer. PL spectra were measured by exciting the sample with the second harmonic (400 nm) of a Ti:sapphire laser (Coherent, Mira 900, repetition rate 76 MHz). The PL emission was spectrally dispersed in a monochromator with a diffraction grating of 30 lines/mm and recorded by a cooled array detector (Andor, iDus 1.7 μm). The excitation density was set using a neutral density filter, and the samples were measured under nitrogen to prevent photodegradation during the experiment. All spectra were corrected for the response of the setup obtained using a calibrated lamp.

Electron Microscopy. TEM and electron diffraction data were collected using a JEOL JEM-2010 at 200 keV. Samples were prepared by drop-casting a diluted PbS-OA CQDs dispersion in hexane onto carbon-coated Cu grids. The ligand exchange was done by immersing the grids in 20 mM solutions of the halide ligands in MeOH for 35 s, followed by a washing in pure MeOH. No annealing was performed after deposition, as we find out in a previous experiment[16] that the annealing procedure does not vary the structural organization of the film.

Energy-dispersive X-ray spectroscopy (EDX) measurements were obtained with a Nova NanoSEM 650 scanning electron microscope.

CQD Solar Cell Fabrication. *Device Fabrication.* Prepatterned FTO glass substrates (13 Ω/sq), were cleaned with detergent, sonicated in acetone and isopropanol and dried in oven at 120 °C for at least 20 min. Then the FTO substrates were treated by O_3 for 20 min. Titanium oxide (TiO_2) sol was prepared by mixing ethanol, titanium(IV) butoxide and HCl (37%) in the ratio 20:2:1, then the sol was spin-casted onto FTO substrates and annealed at 450 °C for 30 min.

PbS CQDs films were deposited in a nitrogen filled glovebox. A layer-by-layer spin-casting method was used for the preparation of the PbS quantum dot films. PbS CQDs with the first excitonic peak of 851 nm (in solution), which correspond to the energy band gap value of 1.46 eV, were used for solar cells fabrication. Oleate-capped PbS CQDs were spin-casted from hexane (10 mg/mL) onto the TiO_2 films. Ligand exchange was performed by subjecting the films to 40 mM TBAI solution, or, 20 mM methanol TBACl solution, or, 20 mM methanol TMAF solution, or, acetonitrile EDT solution (with concentration of 0.01% by volume) for about 35 s. After deposition spin-drying was used to remove the residuals of the ligands solutions. The ligand-exchanged films were washed twice with methanol or once with acetonitrile for the halide- and EDT-treated films, respectively. The cycle of deposition of the oleate-capped PbS CQDs, ligand exchange and washing was repeated 12 times for TBAI-treated layer and four times for p-type layers (EDT, TBACl, or TMAF). The halide-treated films of PbS CQDs were annealed at 90 °C for 25 min to remove the residuals of methanol and to improve the films quality.

The devices were finalized by thermal evaporation of 5 nm of MoO_3 and 80 nm gold under the pressure of 4×10^{-8} mBar at a rate of 0.1 Å/s for MoO_3 and 0.5−2 Å/s for gold. The device area was defined by the overlap of FTO and Au electrodes, which is 0.16 cm^2.

Current−Voltage Characterization. CQD solar cells were measured in the nitrogen filled glovebox under simulated AM1.5 G solar illumination, using a Steuernagel Solar constant 1200 metal halide lamp set to 100 mW/cm^2 intensity and a Keithley 2400 source-meter. Light intensity was calibrated using a monocrystalline silicon solar cell (WRVS reference cell, Fraunhofer ISE). For efficiency calculations, the illuminated area was confined by a shadow mask (0.10 cm^2) to avoid any edge effects. The temperature was set to 295 K and controlled by a nitrogen gas flow through a liquid nitrogen bath.

External Quantum Efficiency (EQE) Measurements. The EQE was measured under monochromatic light at short circuit conditions. For the source of white light a 250 W quartz tungsten halogen lamp (6334NS, Newport) with lamp housing (67009, Newport) was used. Narrow bandpass filters (Thorlabs) with a full width half-maximum (fwhm) of 10 ± 2 nm from 400 to 1300 nm and a fwhm of 12 ± 2.4 nm from 1300 to 1400 nm were used for monochromatic light. The light intensity was determined by calibrated PD300 and PD300IR

DOI: 10.1021/acsanm.8b01696
ACS Appl. Nano Mater. 2018, 1, 6882−6889

photodiodes (Ophir Optics) for visible and infrared parts of the spectrum, respectively.

■ ASSOCIATED CONTENT

Supporting Information

The Supporting Information is available free of charge on the ACS Publications website at DOI: 10.1021/acsanm.8b01696.

Materials characterization (TEM, electron diffraction, PL, and EDX spectra), extra information on fluoride-treated PbS CQD FETs and performance parameters of CQD solar cells (PDF)

■ AUTHOR INFORMATION

Corresponding Author

*Email: m.a.loi@rug.nl.

ORCID

Dmitry N. Dirin: 0000-0002-5187-4555

Maksym V. Kovalenko: 0000-0002-6396-8938

Maria A. Loi: 0000-0002-7985-7431

Notes

The authors declare no competing financial interest.

■ ACKNOWLEDGMENTS

The authors are thankful to A. Kamp and T. Zaharia for the technical support. S. Adjokatse and G. ten Brink are acknowledged for the EDX measurements. Bart Kooi is acknowledged for the access to the TEM. The Groningen team is grateful for the financial support of the European Research Council (ERC Starting Grant "Hy-SPOD" No. 306983) and Dieptestrategie program from Zernike Institute for Advanced Materials.

■ REFERENCES

(1) Talapin, D. V.; Lee, J.-S.; Kovalenko, M. V.; Shevchenko, E. V. Prospects of Colloidal Nanocrystals for Electronic and Optoelectronic Applications. *Chem. Rev.* **2010**, *110*, 389−458.

(2) Kagan, C. R.; Lifshitz, E.; Sargent, E. H.; Talapin, D. V. Building Devices from Colloidal Quantum Dots. *Science* **2016**, *353*, aac5523−aac5523.

(3) Kovalenko, M. V.; Scheele, M.; Talapin, D. V. Colloidal Nanocrystals with Molecular Metal Chalcogenide Surface Ligands. *Science* **2009**, *324*, 1417−1420.

(4) Fafarman, A. T.; Koh, W.; Diroll, B. T.; Kim, D. K.; Ko, D.-K.; Oh, S. J.; Ye, X.; Doan-Nguyen, V.; Crump, M. R.; Reifsnyder, D. C.; Murray, C. B.; Kagan, C. R. Thiocyanate-Capped Nanocrystal Colloids: Vibrational Reporter of Surface Chemistry and Solution-Based Route to Enhanced Coupling in Nanocrystal Solids. *J. Am. Chem. Soc.* **2011**, *133*, 15753−15761.

(5) Nag, A.; Kovalenko, M. V.; Lee, J.-S.; Liu, W.; Spokoyny, B.; Talapin, D. V. Metal-Free Inorganic Ligands for Colloidal Nanocrystals: S^{2-}, HS^{-}, Se^{2-}, HSe^{-}, Te^{2-}, HTe^{-}, TeS_3^{2-}, OH^{-} and NH_2^{-} as Surface Ligands. *J. Am. Chem. Soc.* **2011**, *133*, 10612−10620.

(6) Tang, J.; Kemp, K. W.; Hoogland, S.; Jeong, K. S.; Liu, H.; Levina, L.; Furukawa, M.; Wang, X.; Debnath, R.; Cha, D.; Chou, K. W.; Fischer, A.; Amassian, A.; Asbury, J. B.; Sargent, E. H. Colloidal-Quantum-Dot Photovoltaics Using Atomic-Ligand Passivation. *Nat. Mater.* **2011**, *10*, 765−771.

(7) Zhang, H.; Jang, J.; Liu, W.; Talapin, D. V. Colloidal Nanocrystals with Inorganic Halide, Pseudohalide, and Halometallate Ligands. *ACS Nano* **2014**, *8*, 7359−7369.

(8) Dirin, D. N.; Dreyfuss, S.; Bodnarchuk, M. I.; Nedelcu, G.; Papagiorgis, P.; Itskos, G.; Kovalenko, M. V. Lead Halide Perovskites and Other Metal Halide Complexes As Inorganic Capping Ligands for Colloidal Nanocrystals. *J. Am. Chem. Soc.* **2014**, *136*, 6550−6553.

(9) Sayevich, V.; Gaponik, N.; Plötner, M.; Kruszynska, M.; Gemming, T.; Dzhagan, V. M.; Akhavan, S.; Zahn, D. R. T.; Demir, H. V.; Eychmüller, A. Stable Dispersion of Iodide-Capped PbSe Quantum Dots for High-Performance Low-Temperature Processed Electronics and Optoelectronics. *Chem. Mater.* **2015**, *27*, 4328−4337.

(10) Lin, Q.; Yun, H. J.; Liu, W.; Song, H.-J.; Makarov, N. S.; Isaienko, O.; Nakotte, T.; Chen, G.; Luo, H.; Klimov, V. I.; Pietryga, J. M. Phase-Transfer Ligand Exchange of Lead Chalcogenide Quantum Dots for Direct Deposition of Thick, Highly Conductive Films. *J. Am. Chem. Soc.* **2017**, *139*, 6644−6653.

(11) Ning, Z.; Voznyy, O.; Pan, J.; Hoogland, S.; Adinolfi, V.; Xu, J.; Li, M.; Kirmani, A. R.; Sun, J. P.; Minor, J.; Kemp, K. W.; Dong, H.; Rollny, L.; Labelle, A.; Carey, G.; Sutherland, B.; Hill, I.; Amassian, A.; Liu, H.; Tang, J.; Bakr, O. M.; Sargent, E. H. Air-Stable n-Type Colloidal Quantum Dot Solids. *Nat. Mater.* **2014**, *13*, 822−828.

(12) Zhitomirsky, D.; Furukawa, M.; Tang, J.; Stadler, P.; Hoogland, S.; Voznyy, O.; Liu, H.; Sargent, E. H. N-Type Colloidal-Quantum-Dot Solids for Photovoltaics. *Adv. Mater.* **2012**, *24*, 6181−6185.

(13) Wanger, D. D.; Correa, R. E.; Dauler, E. A.; Bawendi, M. G. The Dominant Role of Exciton Quenching in PbS Quantum-Dot-Based Photovoltaic Devices. *Nano Lett.* **2013**, *13*, 5907−5912.

(14) Ibáñez, M.; Hasler, R.; Liu, Y.; Dobrozhan, O.; Nazarenko, O.; Cadavid, D.; Cabot, A.; Kovalenko, M. V. Tuning p-Type Transport in Bottom-Up-Engineered Nanocrystalline Pb Chalcogenides Using Alkali Metal Chalcogenides as Capping Ligands. *Chem. Mater.* **2017**, *29*, 7093−7097.

(15) Chuang, C.-H. M.; Brown, P. R.; Bulović, V.; Bawendi, M. G. Improved Performance and Stability in Quantum Dot Solar Cells through Band Alignment Engineering. *Nat. Mater.* **2014**, *13*, 796−801.

(16) Balazs, D. M.; Dirin, D. N.; Fang, H.-H.; Protesescu, L.; ten Brink, G. H.; Kooi, B. J.; Kovalenko, M. V.; Loi, M. A. Counterion-Mediated Ligand Exchange for PbS Colloidal Quantum Dot Superlattices. *ACS Nano* **2015**, *9*, 11951−11959.

(17) Weidman, M. C.; Yager, K. G.; Tisdale, W. A. Interparticle Spacing and Structural Ordering in Superlattice PbS Nanocrystal Solids Undergoing Ligand Exchange. *Chem. Mater.* **2015**, *27*, 474−482.

(18) Zhang, Z.; Yang, J.; Wen, X.; Yuan, L.; Shrestha, S.; Stride, J. A.; Conibeer, G. J.; Patterson, R. J.; Huang, S. Effect of Halide Treatments on PbSe Quantum Dot Thin Films: Stability, Hot Carrier Lifetime, and Application to Photovoltaics. *J. Phys. Chem. C* **2015**, *119*, 24149−24155.

(19) Woo, J. Y.; Ko, J.-H.; Song, J. H.; Kim, K.; Choi, H.; Kim, Y.-H.; Lee, D. C.; Jeong, S. Ultrastable PbSe Nanocrystal Quantum Dots via in Situ Formation of Atomically Thin Halide Adlayers on PbSe(100). *J. Am. Chem. Soc.* **2014**, *136*, 8883−8886.

(20) Brown, P. R.; Kim, D.; Lunt, R. R.; Zhao, N.; Bawendi, M. G.; Grossman, J. C.; Bulović, V. Energy Level Modification in Lead Sulfide Quantum Dot Thin Films through Ligand Exchange. *ACS Nano* **2014**, *8*, 5863−5872.

(21) Christe, K. O.; Wilson, W. W.; Wilson, R. D.; Bau, R.; Feng, J. A. Syntheses, Properties, and Structures of Anhydrous Tetramethylammonium Fluoride and Its 1:1 Adduct with Trans-3-Amino-2-Butenenitrile. *J. Am. Chem. Soc.* **1990**, *112*, 7619−7625.

(22) Li, H.-Y.; Sun, H.; DiMagno, S. G. Tetra-n-Butylammonium Fluoride. In *Encyclopedia of Reagents for Organic Synthesis*; John Wiley & Sons: Chichester, U.K., 2007.

(23) Balazs, D. M.; Nugraha, M. I.; Bisri, S. Z.; Sytnyk, M.; Heiss, W.; Loi, M. A. Reducing Charge Trapping in PbS Colloidal Quantum Dot Solids. *Appl. Phys. Lett.* **2014**, *104*, 112104.

(24) Ihly, R.; Tolentino, J.; Liu, Y.; Gibbs, M.; Law, M. The Photothermal Stability of PbS Quantum Dot Solids. *ACS Nano* **2011**, *5*, 8175−8186.

(25) Kirmani, A. R.; Sheikh, A. D.; Niazi, M. R.; Haque, M. A.; Liu, M.; de Arquer, F. P. G.; Xu, J.; Sun, B.; Voznyy, O.; Gasparini, N.; Baran, D.; Wu, T.; Sargent, E. H.; Amassian, A. Overcoming the Ambient Manufacturability-Scalability-Performance Bottleneck in

DOI: 10.1021/acsanm.8b01696
ACS Appl. Nano Mater. 2018, 1, 6882−6889

Colloidal Quantum Dot Photovoltaics. *Adv. Mater.* **2018**, *30*, 1801661.
(26) Sun, H.; DiMagno, S. G. Anhydrous Tetrabutylammonium Fluoride. *J. Am. Chem. Soc.* **2005**, *127*, 2050−2051.
(27) Moreels, I.; Lambert, K.; Smeets, D.; De Muynck, D.; Nollet, T.; Martins, J. C.; Vanhaecke, F.; Vantomme, A.; Delerue, C.; Allan, G.; Hens, Z. Size-Dependent Optical Properties of Colloidal PbS Quantum Dots. *ACS Nano* **2009**, *3*, 3023−3030.
(28) Shulga, A. G.; Piveteau, L.; Bisri, S. Z.; Kovalenko, M. V.; Loi, M. A. Double Gate PbS Quantum Dot Field-Effect Transistors for Tuneable Electrical Characteristics. *Adv. Electron. Mater.* **2016**, *2*, 1500467.
(29) Choi, H.; Ko, J. H.; Kim, Y. H.; Jeong, S. Steric-Hindrance-Driven Shape Transition in PbS Quantum Dots: Understanding Size-Dependent Stability. *J. Am. Chem. Soc.* **2013**, *135*, 5278−5281.
(30) Oh, S. J.; Wang, Z.; Berry, N. E.; Choi, J.-H.; Zhao, T.; Gaulding, E. A.; Paik, T.; Lai, Y.; Murray, C. B.; Kagan, C. R. Engineering Charge Injection and Charge Transport for High Performance PbSe Nanocrystal Thin Film Devices and Circuits. *Nano Lett.* **2014**, *14*, 6210−6216.
(31) Balazs, D. M.; Bijlsma, K. I.; Fang, H.-H.; Dirin, D. N.; Döbeli, M.; Kovalenko, M. V.; Loi, M. A. Stoichiometric Control of the Density of States in PbS Colloidal Quantum Dot Solids. *Sci. Adv.* **2017**, *3*, No. eaao1558.
(32) Whitham, K.; Yang, J.; Savitzky, B. H.; Kourkoutis, L. F.; Wise, F.; Hanrath, T. Charge Transport and Localization in Atomically Coherent Quantum Dot Solids. *Nat. Mater.* **2016**, *15*, 557−563.
(33) Evers, W. H.; Schins, J. M.; Aerts, M.; Kulkarni, A.; Capiod, P.; Berthe, M.; Grandidier, B.; Delerue, C.; van der Zant, H. S. J.; van Overbeek, C.; Peters, J. L.; Vanmaekelbergh, D.; Siebbeles, L. D. A. High Charge Mobility in Two-Dimensional Percolative Networks of PbSe Quantum Dots Connected by Atomic Bonds. *Nat. Commun.* **2015**, *6*, 8195.
(34) Kim, D.; Kim, D.-H.; Lee, J.-H.; Grossman, J. C. Impact of Stoichiometry on the Electronic Structure of PbS Quantum Dots. *Phys. Rev. Lett.* **2013**, *110*, 196802.
(35) Han, L.; Balazs, D. M.; Shulga, A. G.; Abdu-Aguye, M.; Ma, W.; Loi, M. A. PbSe Nanorod Field-Effect Transistors: Room- and Low-Temperature Performance. *Adv. Electron. Mater.* **2018**, *4*, 1700580.
(36) Christe, K. O.; Wilson, W. W. Reaction of the Fluoride Anion with Acetonitrile, Chloroform and Methylene Chloride. *J. Fluorine Chem.* **1990**, *47*, 117−120.
(37) Speirs, M. J.; Dirin, D. N.; Abdu-Aguye, M.; Balazs, D. M.; Kovalenko, M. V.; Loi, M. A. Temperature Dependent Behaviour of Lead Sulfide Quantum Dot Solar Cells and Films. *Energy Environ. Sci.* **2016**, *9*, 2916−2924.
(38) Speirs, M. J.; Balazs, D. M.; Dirin, D. N.; Kovalenko, M. V.; Loi, M. A. Increased Efficiency in pn-Junction PbS QD Solar Cells via NaHS Treatment of the p-Type Layer. *Appl. Phys. Lett.* **2017**, *110*, 103904.
(39) Kirmani, A. R.; García de Arquer, F. P.; Fan, J. Z.; Khan, J. I.; Walters, G.; Hoogland, S.; Wehbe, N.; Said, M. M.; Barlow, S.; Laquai, F.; Marder, S. R.; Sargent, E. H.; Amassian, A. Molecular Doping of the Hole-Transporting Layer for Efficient, Single-Step-Deposited Colloidal Quantum Dot Photovoltaics. *ACS Energy Lett.* **2017**, *2*, 1952−1959.
(40) Tang, J.; Liu, H.; Zhitomirsky, D.; Hoogland, S.; Wang, X.; Furukawa, M.; Levina, L.; Sargent, E. H. Quantum Junction Solar Cells. *Nano Lett.* **2012**, *12*, 4889−4894.
(41) Speirs, M. J.; Balazs, D. M.; Fang, H.-H.; Lai, L.-H.; Protesescu, L.; Kovalenko, M. V.; Loi, M. A. Origin of the Increased Open Circuit Voltage in PbS−CdS Core−shell Quantum Dot Solar Cells. *J. Mater. Chem. A* **2015**, *3*, 1450−1457.
(42) Hines, M. A.; Scholes, G. D. Colloidal PbS Nanocrystals with Size-Tunable Near-Infrared Emission: Observation of Post-Synthesis Self-Narrowing of the Particle Size Distribution. *Adv. Mater.* **2003**, *15*, 1844−1849.

DOI: 10.1021/acsanm.8b01696
ACS Appl. Nano Mater. 2018, 1, 6882−6889